

1 **Trends and ENSO-related variability in Atlantic tropical cyclone intensity**
2 **and intensification**

3 Michael K. Tippett^a and Suzana J. Camargo^b

4 ^a *Department of Applied Physics and Applied Mathematics, Columbia University, New York, New*
5 *York*

6 ^b *Columbia Climate School, Columbia University, New York, New York*

7 *Corresponding author: M. K. Tippett, mkt14@columbia.edu*

8 ABSTRACT: This study examined trends and ENSO-related variability in Atlantic tropical cy-
9 clone intensity, focusing on 24-h intensification, lifetime maximum intensity (LMI), and rapid
10 intensification (RI) in best-track data during the period 1982–2024. Previous studies considered
11 trends and ENSO influences separately, reporting upward trends in intensity and more cases of RI
12 during La Niña conditions. Here we extended and built upon prior work by including data through
13 2024, assessing the impact of ENSO on LMI and 24-h intensification, and analyzing a new storm
14 metric called lifetime maximum 24-h intensification (LM24I). The statistical methods employed
15 here improve upon previous ones by correctly assessing uncertainty and statistical significance,
16 simultaneously estimating trends and ENSO-related variability, and addressing problems arising
17 from the 5-kt discretization of best-track intensity data. Quantile and logistic regression were
18 employed extensively. The main findings include the following: Prior estimates of intensification
19 trends were overconfident, and including recent data reduces prior estimates of trends in intensifi-
20 cation, RI frequency, and LMI. The distribution of LM24I shows significant upward trends of 3–5
21 kt per decade in its top quantiles and broad increases of 2–5 kt per degree of Niño-3.4 cooling.
22 During La Niña conditions, the frequencies of RI events and RI storms increase, and the distribu-
23 tions of 24-h intensification and LMI show previously unreported broad and significant increases.
24 Directions for future research include applying the same approaches to other intensity metrics,
25 basins, and model output, and leveraging ENSO predictability for seasonal intensity prediction.

26 SIGNIFICANCE STATEMENT: This study examined how the intensity (wind speed) of topical
27 cyclones in the Atlantic has changed over time and how it varies with El Niño and La Niña.
28 In terms of trends, the most intense storms are becoming stronger and the most extreme rapid
29 intensification is becoming more frequent. During La Niña conditions, intensification rates are
30 higher and hurricanes are stronger. Use of better statistical techniques and additional data resulted
31 in reduced upward trends compared to prior estimates and a more comprehensive picture of the
32 impacts of El Niño and La Niña on Atlantic tropical cyclone intensity.

33 **1. Introduction**

34 Tropical cyclones are among the most destructive natural disasters, causing damage and loss of
35 life through storm surge, high winds, and heavy rainfall. The hazard posed by tropical cyclones can
36 be characterized by a range of features, including their track, size, translation speed, and intensity.
37 Of these characteristics, maximum sustained wind speed (intensity) receives particular attention
38 and is a commonly used metric for classifying storm severity, though other intensity measures (e.g.,
39 surface pressure; Klotzbach et al. 2020) and factors (e.g., storm size; Zhai and Jiang 2014) may
40 better determine the impact of a particular storm. This study focuses on two aspects of Atlantic
41 tropical cyclone intensity: trends and ENSO-related variability. Observed long-term trends in
42 tropical cyclone intensity and intensification provide information for what to expect in a changing
43 climate as well as validation for models and theory (Knutson et al. 2019, 2020; Camargo et al.
44 2023). ENSO-related variability in tropical cyclone behavior is especially relevant on interannual
45 timescales since ENSO is the primary source of seasonal predictability.

46 Upward tropical cyclone intensity trends are expected in a warming climate on the basis of
47 potential intensity theory (e.g., Sobel et al. 2016) and high-resolution models (e.g., Knutson et al.
48 2010). Kossin et al. (2013, their Figs. 5 and 10) found positive trends in quantiles above the
49 median of lifetime maximum intensity (LMI) for Atlantic storms that reached hurricane strength in
50 Advanced Dvorak Technique Hurricane Satellite (ADT-HURSAT) data and in best-track data over
51 the period 1982–2009. Over the same 1982–2009 period, Bhatia et al. (2019, their Fig. 2c) found
52 statistically significant positive trends in annual quantiles of Atlantic basin 24-h intensification
53 above the 0.6 quantile (3 kt decade⁻¹ in the 0.95 quantile) and negative significant trends in
54 quantiles below the 0.45 quantile using International Best Track Archive for Climate Stewardship

55 (IBTrACS) data. Significant trends in the quantiles of 24-h intensification from ADT-HURSAT data
56 were limited to the most extreme quantiles — positive in the 0.9 and 0.95 quantile (4 kt decade^{-1}),
57 and negative in the 0.05 and 0.1 quantiles (Bhatia et al. 2019, their Fig. 2d). Bhatia et al. (2019, their
58 Fig. 3b) also found a significant upward trend in the frequency of rapid intensification (RI; 24-h
59 intensification greater than 30 kt) in the Atlantic basin. Based on bias-corrected model simulations,
60 they concluded “natural variability cannot explain the magnitude of the observed upward trend.”
61 Balaguru et al. (2018) examined Atlantic storm intensification at sub-basin resolutions over the
62 period 1986–2015 and found a significant upward trend ($3.8 \text{ kt decade}^{-1}$) in the 0.95 annual
63 quantile of 24-h intensification east of 60°W and no significant trend in intensification to the west.
64 They speculated that the upward intensification trend in the eastern region was due to the Atlantic
65 Multidecadal Oscillation (AMO) transitioning from a negative to a positive phase over the same
66 period. In another regional analysis, Balaguru et al. (2022) found statistically significant increases
67 in the average 24-h intensification of storms near the U.S. Atlantic coast for the period 1979–2018,
68 but not for storms near the Gulf coast, though RI frequency increased in both regions.

69 ENSO influences Atlantic tropical cyclones through changes in vertical shear and stability that
70 make conditions less favorable for storm formation and intensification during El Niño and more
71 favorable during La Niña conditions (Gray 1984; Bove et al. 1998; Tang and Neelin 2004; Klotzbach
72 2011). Jagger and Elsner (2009) examined the influence on ENSO on maxima of near-coastal
73 tropical cyclone intensity interpolated from HURDAT and found that the average and 0.5–0.9
74 quantiles increased as the Southern Oscillation Index increased toward La Niña-like conditions.
75 Klotzbach (2012, their Fig. 2) stratified RI events by ENSO state during the period 1974–2010
76 and found that nearly three times as many RI events occurred in La Niña years as in El Niño
77 years for a range of RI thresholds (intensification of at least 25, 30, 35, or 40 kt in a 24-h storm
78 period). Klotzbach (2012, their Table 2) also found that the frequency of RI storms (storms that
79 undergo RI at some point during their lifetime) was higher during La Niña years than during El
80 Niño years. Wang et al. (2017, their Table 1) found that over the period 1950–2104 the number
81 of North Atlantic RI events (30 kt threshold) was significantly correlated ($r = -0.45$) with the
82 June–November average Niño-3.4 index. Klotzbach et al. (2022, their table S4) found a negative
83 correlation (-0.41) between 50-kt RI event numbers and the ENSO Longitude Index (ELI; Williams
84 and Patricola 2018) over the recent period 1990–2021.

85 Questions remain regarding trends and ENSO-related variability in Atlantic tropical cyclone
86 intensification. For instance, Klotzbach (2012) left open the question of whether the higher
87 number of RI events during La Niña years was due to increased likelihood of RI during La Niña
88 years or due to simply more storms and more opportunities for RI (annual numbers of storms and
89 RI events are significantly correlated; Wang et al. 2017, their Table 4). Although RI is known to
90 be related to LMI (e.g., Lee et al. 2016), to date, the relation of ENSO with LMI has not been
91 examined. Previous trend results may be specific to the period examined. For instance, although
92 Bhatia et al. (2019) found trends in RI frequency, Wang et al. (2017) considered the longer period
93 1950–2014 and noted no long-term trend in RI numbers. Likewise Klotzbach et al. (2022, their
94 table S2) found no significant trends in Atlantic RI events (30 kt and 50 kt thresholds) over the
95 recent period 1990–2021. Whether trends are limited to a past period or whether they extend to
96 present is an important consideration in deciding if trend information might be used to anticipate
97 future conditions.

98 There are also methodological questions. For instance, accurately assessing statistical signifi-
99 cance is critical when the signals in question are modest. Therefore, an issue of interest is whether
100 the ad hoc procedure in Bhatia et al. (2019, 2022) that added random noise to the observations
101 to mimic observational error accurately captured the uncertainty of trend estimates. Some trend
102 analysis first computed annual quantiles for each year and then fit trends in those annual quantiles
103 by ordinary least squares (OLS) regression (e.g., Balaguru et al. 2018; Bhatia et al. 2019). Other
104 analysis used quantile regression which pools all the data in the fitting procedure and computes
105 trends via least asymmetric absolute loss (e.g., Jagger and Elsner 2009; Elsner and Jagger 2013;
106 Kossin et al. 2013). To date the theoretical or practical differences between these approaches have
107 not been investigated in the context of tropical cyclone trends. A similar issue arises in the analysis
108 of frequency trends (e.g., frequency of RI events or frequency of RI storms). One approach is
109 to compute the annual proportion for each year first and then to compute their trends by OLS
110 regression (e.g., Bhatia et al. 2019). On the other hand, logistic regression, which is commonly
111 used in RI forecast applications (e.g., Knaff et al. 2018), is specifically designed for analysis of
112 frequencies and has the advantage of taking account of all the event data in the fitting process. As
113 with quantile regression, the theoretical or practical differences between these approaches have not
114 been examined in the context of RI trends. Previous analysis has considered trends and ENSO

115 separately. Accounting for ENSO variability might reduce the uncertainty in trend estimates. A
116 final methodological point is that best-track intensity data are recorded in 5 kt increments. Statis-
117 tical methods that assume continuous random variables tend to perform poorly with discrete data,
118 which is an issue whose implications have not been investigated in the context of tropical cyclone
119 intensification.

120 In this paper we have addressed several of the questions and gaps identified above. With regard
121 to ENSO-related variability, we extended the studies of Klotzbach (2012) and Wang et al. (2017)
122 which found more RI events during cool ENSO conditions, to consider the question of whether
123 such increases are simply due to an increase in tropical storm activity (more 24-h periods) during
124 cool ENSO conditions or whether RI events are inherently more likely. We also examined the
125 impact of ENSO state on 24-h intensification beyond RI and on LMI. We explored whether trends
126 may be specific to past periods by (i) using data through 2024, and (ii) repeating some analysis with
127 start years of 1950, 1960, 1970, and 1982. The 1982 start year was chosen to match that in the trend
128 studies of Kossin et al. (2013) and Bhatia et al. (2019). We used regression methods that permit
129 treating trends and ENSO-related variability simultaneously. We focused on two methodological
130 issues: whether adding random noise to the observations results in accurate assessments of trend
131 uncertainty and statistical significance, and how discrete intensity data affect the calculation of
132 quantiles and quantile regression. We also discussed differences between OLS and advanced
133 (quantile and logistic) regression methods and compared results in a few cases.

134 The paper is organized as follows. Data and methods are described in Section 2, including
135 logistic and quantile regression. The impact of quantized best-track intensity data on statistical
136 analysis is examined in Section 3 along with recommendations on the use of jitter. Trends and
137 ENSO-related variability are reported in Section 4. Results are summarized and directions for
138 future work are provided in Section 5.

139 **2. Data and methods**

140 *a. Data*

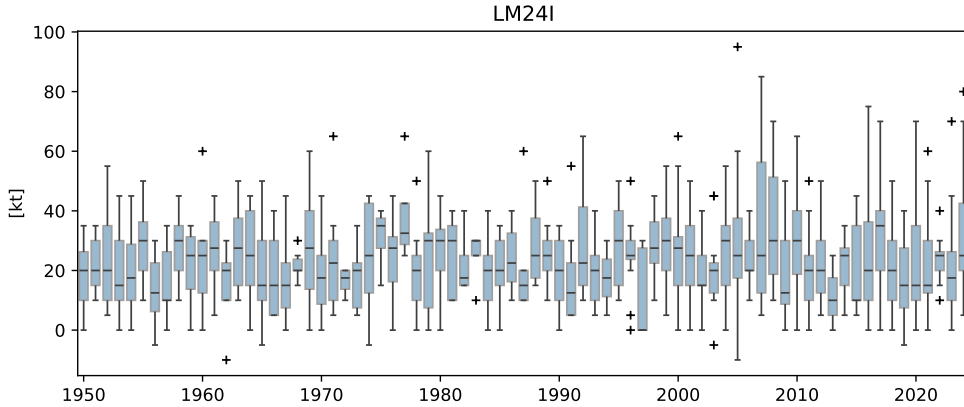
141 Most of the analysis used the period 1982–2024. For composites, the early period was defined
142 to be 1982–2002 (21 years) and the late period to be 2003–2024 (22 years). For the quantile

143 regression analysis, we repeated the calculations using as start years: 1950, 1960, and 1970 to see
144 the robustness of the results and their sensitivity to period.

145 The ENSO state was characterized by the August–October (ASO) Niño-3.4 index, which is the
146 average of sea surface temperature (SST) in the region 170°W–120°W, 5°S–5°N (Barnston et al.
147 1997). SST data 1950–2024 were taken from ERSSTv5 (Huang et al. 2017). For composites, El
148 Niño (warm) and La Niña (cool) years were defined to be ones whose ASO Niño-3.4 index values
149 were in the upper and lower quartiles, respectively, of the data (Hanley et al. 2003). The thresholds
150 for the period 1982–2024 are -0.63°C and $+0.54^{\circ}\text{C}$, expressed as anomalies with respect to the
151 mean over the period. These thresholds resulted in 11 El Niño years: 1982, 1986, 1987, 1991,
152 1994, 1997, 2002, 2004, 2009, 2015, and 2023 (also classified as ASO El Niño by CPC) and 11
153 La Niña years: 1983, 1988, 1995, 1998, 1999, 2007, 2010, 2011, 2020, 2021, and 2022 (also
154 classified as ASO La Niña by CPC).¹ The average difference between warm and cool year values
155 of ASO Niño-3.4 is 2.2°C .

156 Atlantic tropical cyclone data 1950–2024 were taken from the International Best Track Archive
157 for Climate Stewardship (IBTrACS, V04r01; Knapp et al. 2010; Gahtan et al. 2024). Values for
158 2024 are provisional and derived from operational data collected in real-time. Intensity values were
159 taken from the USA_WIND entries. The storm data were filtered to retain entries: at 0, 6, 12, and
160 18 UTC, during June–November, over ocean ($\text{DIST2LAND} > 0$), and with Saffir-Simpson ratings
161 of “tropical storm” and greater ($\text{USA_SSHS} \geq 0$). This filtering leaves only 6-hourly snapshots with
162 intensities of 35 kt or greater and US_STATUS values of tropical storm and hurricane. Measures of
163 tropical cyclone intensity and intensification considered were: LMI (lifetime maximum intensity;
164 one value per storm), 24-h intensification (all over-lapping 24-h storm periods), RI events (yes/no
165 per 24-h period), and RI storms (yes/no per storm) using RI thresholds of 20 kt to 40 kt by 5 kt.
166 We also analyzed a new quantity called lifetime maximum 24-h intensification (LM24I; one value
167 per storm) shown in Fig. 1. This quantity is negative for seven storms (less than 1% of the total).
168 The most recent case was Melissa which evolved in October of 2019 from an extratropical low to
169 a subtropical storm and then to a tropical storm. Melissa (2019) only weakened during its time as
170 a tropical storm, and therefore its LM24I is negative (-5 kt).

¹https://origin.cpc.ncep.noaa.gov/products/analysis_monitoring/ensostuff/ONI_v5.php



171 FIG. 1. Boxplots of lifetime maximum 24-h intensification (LM24I) values by year for Atlantic tropical storms
 172 and hurricanes. The box covers the interquartile range (IQR) with a line that marks the median. Whiskers extend
 173 to the smallest and largest data points within 1.5 times the IQR from the lower and upper quartiles, respectively.
 174 Plus signs are values outside this range.

175 *b. Methods*

176 Data were stratified into early/late periods and warm/cool ENSO years. The statistical signifi-
 177 cance of differences between samples from early and late periods, as well as from warm and cool
 178 ENSO years, was assessed using the Kolmogorov-Smirnov (KS) test. Distributions were plotted
 179 as histograms (bins with width of 5 kt, centered on multiples of five), kernel smoothed probability
 180 density functions, and return level plots that use the approximate return period $-1/\log f$ where
 181 f is the cumulative frequency (DelSole and Tippett 2022). Return level plots contain the same
 182 information as cumulative distribution plots but provide a clearer representation of the behavior of
 183 extreme values by replacing small exceedance probabilities with large return periods and using a
 184 log scale.

Differences in occurrence counts (e.g., number of RI events or RI storms) between early/late periods and warm/cool ENSO years were tabulated in 2×2 contingency tables. For example, a 2×2 table for RI events and warm/cool years has the form:

	RI	no-RI
Warm	a	b
Cool	c	d

185 where a , b , c , and d are the number of cases. The odds ratio is a standard measure of association
 186 for 2×2 contingency tables and is used to measure the dependence between two variables, in this
 187 example, ENSO state and RI occurrence. The odds of RI during warm and cool conditions are
 188 a/b and c/d , respectively. The odds ratio (cool/warm) is cb/ad . Values of the odds ratio greater
 189 than one indicate more frequent RI events during cool conditions, and values near one (equal odds)
 190 favor deciding no association. Fisher's exact test was used to compute the statistical significance
 191 of contingency tables and confidence intervals for the odds ratio.

192 Logistic regression relates the log odds of an event to a linear function of covariates (predictors
 193 variables). Here logistic regression was applied to occurrence of RI events (yes/no per 24-h period),
 194 and RI storms (yes/no per storm), and the covariates were time (in decades) and the Niño-3.4 index.
 195 The logistic regression has the form

$$\log \text{ odds} = \log \left(\frac{p}{1-p} \right) = \beta_0 + \beta_{\text{time}} \text{ time} + \beta_{\text{Niño-3.4}} \text{ Niño-3.4},$$

196 where p is the probability of the event conditional on time and the Niño-3.4 index. Logistic
 197 regression is an alternative to computing annual proportions and fitting an OLS regression to those
 198 annual values. Advantages of logistic regression include: the resulting proportions are bounded
 199 between zero and one; confidence intervals are more accurate; sensitivity to outliers is reduced;
 200 the OLS assumption of uniform variance residuals (violated for proportions near zero or one) is
 201 avoided; the fitting procedure sees all the data and accounts for different numbers of events per
 202 year. To illustrate the last point, consider an intercept-only regression (horizontal line) which
 203 computes the climatological frequency of RI events. The logistic regression approach correctly
 204 computes the frequency as the number of occurrences divided by the number of RI opportunities.
 205 The OLS approach, however, first computes the frequency for each year and then averages those
 206 annual frequencies, which gives an incorrect result when the number of RI opportunities varies
 207 from year to year.

208 Logistic regression coefficient values are the log odds change for a unit change in the covariate.
 209 The corresponding probability change is a nonlinear function of the odds change, which means that
 210 the change from a baseline probability for a unit change in covariate depends on both the logistic
 211 regression coefficient and the baseline probability value. To show the nonlinear dependence of the

212 logistic regression probability on its covariates, and we plotted the probability as function of one
213 covariate and held the other covariate fixed to its average value.

214 Quantile regression models the quantiles of a quantity as a linear function of covariates. Here we
215 applied quantile regression to 24-h intensification, LM24I, and LMI and used as covariates time
216 (in decades) and the Niño-3.4 index. Namely, the conditional quantile Y_τ was modeled as

$$Y_\tau = \beta_{0,\tau} + \beta_{\text{time},\tau} \text{time} + \beta_{\text{Niño-3.4},\tau} \text{Niño-3.4}. \quad (1)$$

217 The conditional τ -quantile of a quantity Y is the threshold so that $\text{Prob}(Y \leq Y_\tau | \text{time}, \text{Niño-3.4}) = \tau$.
218 For instance, the probability level $\tau = 0.5$ corresponds to the conditional median. The quantile
219 regression coefficients were computed separately for each probability level τ by optimizing asym-
220 metric absolute loss (AAL; Koenker and Bassett 1978). Quantile regression is an alternative to
221 computing annual quantiles for each year separately and then fitting an OLS regression to those
222 values. As mentioned in the Introduction, both approaches have been used to analyze trends in
223 tropical cyclone intensity. Like logistic regression, quantile regression has the advantage of using
224 the entire dataset in the fitting process and accounts for differing numbers of events from one year
225 to another. Differing annual numbers of events result in differing levels of uncertainty in the annual
226 quantiles, a factor that is neglected in the subsequent OLS regression, which assumes constant
227 residual variance. Becker and Tippett (2024) compared quantile regression and OLS regression
228 of annual quantiles of December–February daily temperature. In that application, the number of
229 samples each year was fixed (February 29 was excluded), but differences between OLS and quantile
230 regression remained because quantile regression optimizes a different cost function (AAL) and that
231 cost function is a function of all the data, not just annual statistics.

232 Best-track TC wind speeds are recorded in discrete 5-knot increments. Such quantized data pose
233 challenges for statistical estimation and inference which often assume samples come from a contin-
234 uous distribution. In the case of quantile regression when data are concentrated in discrete levels,
235 the quantile regression optimization may be unstable or biased, especially for extreme quantiles.
236 Likewise, the KS test, which is used to decide if samples come from different distributions, as-
237 sumes a continuous cumulative distribution function. Discrete data reduce the test’s sensitivity and
238 produce inaccurate p-values. Adding small random noise, or *jitter*, fills in “gaps” where there are
239 no values and results in data with an approximately continuous distribution which better matches

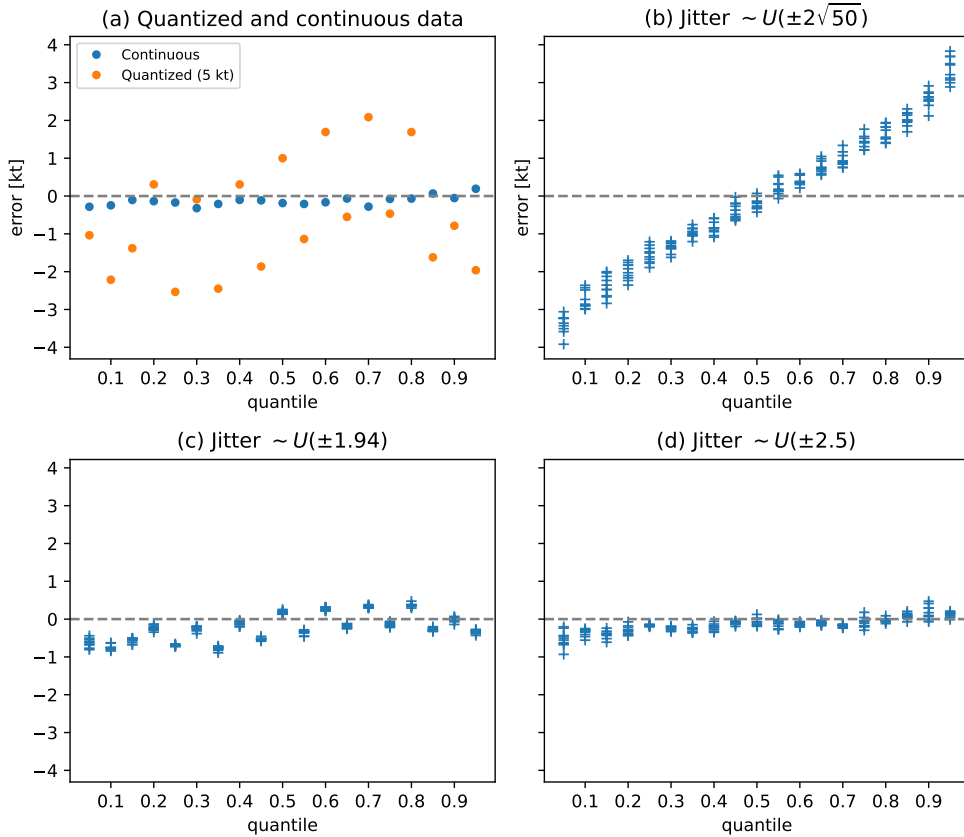
240 the assumptions underlying many parametric and nonparametric statistical methods. The issue of
241 jitter has been discussed in the statistics literature in the context of count data (Machado and Silva
242 2005). Tippett et al. (2016) used jitter in the analysis of tornado counts. Here we added jitter to
243 the intensity data by adding random numbers uniformly distributed on the interval ± 2.5 kt, which
244 matches the 5 kt quantization. Regression coefficients, confidence intervals, and p-values were
245 averaged over 100 realizations of the jitter. Since this issue does not seem to have been addressed
246 in the tropical cyclone literature, we examine the impact of jittering on quantile estimates and
247 quantile regression in Section 3.

248 3. Quantization and jitter

249 When dealing with discrete data, the statistics literature often suggests adding random noise
250 (jitter) whose support (values with non-zero probability) fill in the gaps (Pearson 1950). Jitter
251 that is uniformly distributed on the interval ± 2.5 kt accomplishes this for best-track intensity data.
252 However, other levels of jitter have been used with tropical cyclone intensity data. Bhatia et al.
253 (2019) added jitter uniformly distributed on the interval $\pm 2\sqrt{50}$ kt to intensity change values.
254 Kossin et al. (2013) added jitter uniformly distributed on the interval ± 1.94 kt (± 1 m/s) to LMI
255 values.

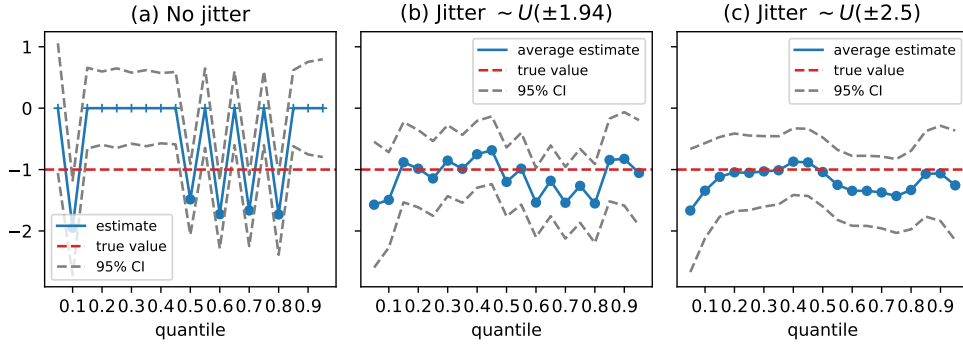
256 a. Computing quantiles

262 To see the impact of these jitter choices on quantile estimates, we generated synthetic normally
263 distributed data with the same sample size (7682), mean (4), and standard deviation (17) as the
264 1982–2024 24-h intensification data. We used synthetic data so that the population values of the
265 quantiles are known. We then computed the sample quantiles of the synthetic data and their error
266 compared to the population quantiles. The magnitude of sample quantile errors was less than
267 0.2 kt (blue dots in Fig. 2a). Repeating the quantile calculation with the same data rounded to
268 the nearest 5 kt (quantized) introduced errors in the quantile estimates which exceed 2 kt (orange
269 dots in Fig. 2a) and are substantially larger than those from sampling variability. Adding jitter
270 uniformly distributed on the interval $\pm 2\sqrt{50}$ kt to the quantized data introduced a systematic bias
271 in the quantiles which is negative for quantiles below the median, positive for quantiles above the
272 median, and larger for more extreme quantiles (Fig. 2b). The reason for this bias is that the variance



257 FIG. 2. Errors of quantile estimates at probability levels 0.05–0.95 by 0.1 for (a) synthetic continuous data
 258 (blue) and the same data quantized to the nearest 5 kt (orange), (b) the quantized data with jitter (random noise)
 259 uniformly distributed on $\pm 2\sqrt{50}$ kt added, (c) the quantized data with jitter uniformly distributed on ± 1.94 kt
 260 added, and (d) the quantized data with jitter uniformly distributed on ± 2.5 added. Panels b, c, and d show the
 261 quantile estimate errors for 10 realizations of the jitter.

273 of a sum of independent random variables is the sum of their variances. Therefore while adding
 274 mean-zero random values leaves the mean unchanged, the variance is increased, which shifts high
 275 quantiles upward and low quantiles downward, as observed here. Too large jitter biases quantile
 276 estimates. Adding jitter uniformly distributed on the interval ± 1.94 kt reduced the quantile errors
 277 compared to those of the quantized data, though they remain noticeable. Too small jitter fails to
 278 fill in gaps in discrete data ($1.94 < 2.5$). Adding jitter uniformly distributed on the interval ± 2.5 kt
 279 matches the gaps in the discrete data and resulted in errors that are comparable on average to those



283 FIG. 3. Quantile regression coefficient estimates (blue lines) from synthetic data (a) without jitter, (b) with
 284 jitter uniformly distributed on the interval ± 1.94 kt, and (c) with jitter uniformly distributed on the interval ± 2.5
 285 kt. The true quantile regression coefficient value is -1 (red dashed line). Dashed gray lines are 95% confidence
 286 intervals. Solid blue circles indicate statistical significance at the 5% level.

280 due to sampling variability (Fig. 2d). The results of the synthetic data experiment support the use
 281 of jitter uniformly distributed on the interval ± 2.5 kt when estimating quantiles of intensity data.

282 *b. Quantile regression*

A problem when applying quantile regression to discrete data is that the conditional quantile (see Eq. 1) is a discontinuous function of its covariates, i.e., it changes from one discrete value to another. To illustrate the consequences of this issue, we applied quantile regression to synthetic data that is the same size as the 1982–2024 24-h intensification data. The synthetic data were generated according to

$$y = -\text{Niño}-3.4 + \text{noise},$$

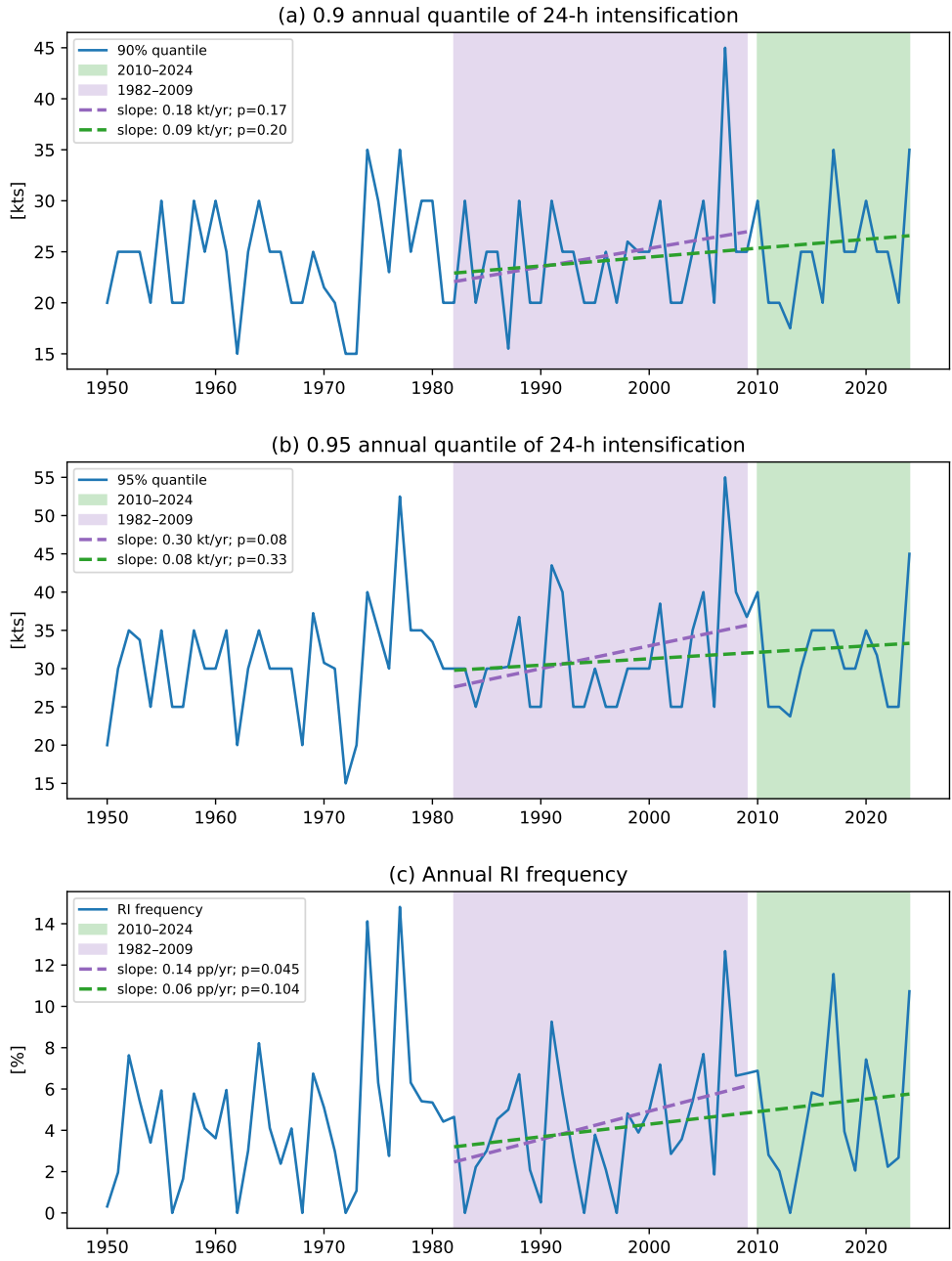
287 where the noise was normally distributed with mean zero and standard deviation 17, and the Niño-
 288 3.4 values were the observed ones. By construction, the population quantiles shift by minus one
 289 for each one degree increase of Niño-3.4. The synthetic data were then rounded to the closest
 290 multiple of 5 and fit by quantile regression. Without jitter, the quantile regression coefficient
 291 estimates show sawtooth behavior and are overly variable (Fig. 3a). The confidence intervals fail
 292 to include the true value. After adding jitter that is uniformly distributed on the interval ± 1.94 kt to
 293 the data, the quantile regression coefficient estimates are closer to their true values but noticeably

294 variable from one probability level to the next, though the confidence intervals include the true
295 value (Fig. 3b). After adding jitter that is uniformly distributed on the interval ± 2.5 kt to the data,
296 the quantile regression coefficient estimates are smoother and relatively close to their true values
297 (Fig. 3c). These results support adding jitter that is uniformly distributed on the interval ± 2.5 kt
298 when applying quantile regression to intensity data.

299 *c. Uncertainty quantification*

300 To quantify the uncertainty of computed trends, Bhatia et al. (2019) added jitter that was uniformly
301 distributed on the interval $\pm 2\sqrt{50}$ kt to each intensity change value, computed the trend in annual
302 quantiles by OLS regression, repeated this process 1000 times, reported the average trend, and
303 considered the 5th and 95th percentiles of the 1000 trends as a 90% confidence interval for the trend.
304 The size of the jitter was chosen based on the typical error of intensity observations. However, the
305 typical purpose of adding jitter, as discussed above, is to address quantization effects rather than
306 simulating observation error or quantifying uncertainty. Since observation error is only one source
307 of trend uncertainty, the procedure fails to provide a complete quantification of uncertainty. For
308 instance, in the case of no error or negligible measurement error, the procedure would result in trend
309 estimates with no uncertainty, which is clearly incorrect. Accounting only for observation error
310 underestimates trend uncertainty. Bootstrapping of residuals is a common method of quantifying
311 the uncertainty of regression coefficients. In this method, residuals of a regression are randomly
312 added to the data, and the regression refit, which is similar in spirit to the Bhatia et al. (2019)
313 procedure. However, observational error does not determine the magnitude of regression residuals.
314 For instance, in the case of no relation between predictors and the predictand y , the variance of the
315 residuals is approximately the variance of y , which is larger than the observation error variance
316 for reliable observations (noise less than signal). In general, the variance of the residuals is
317 approximately the fraction of unexplained variance $(1 - r^2)$ times the climatological variance of y .

321 To see the extent to which the procedure of Bhatia et al. (2019) underestimates the uncertainty of
322 trends, we examined the annual 0.9 and 0.95 quantiles of 24-h intensification data over the period
323 1950–2024 (Fig. 4a, b). Following the procedure of Bhatia et al. (2019, their Fig. 2c), we computed
324 trends of 0.19 kt yr^{-1} and 0.28 kt yr^{-1} over the period 1982–2009 with 90% interval of $[0.095,$
325 $0.28] \text{ kt yr}^{-1}$ and $[0.18, 0.39] \text{ kt yr}^{-1}$, respectively, for the trends of the 0.9 and 0.95 quantile,



318 FIG. 4. Time series of (a) 0.9, (b) 0.95 annual quantiles of Atlantic 24-h intensification, and (c) annual Atlantic
 319 RI frequency 1950–2024. Values during the periods 1982–2009 and 1982–2024 are fit to linear trends by OLS
 320 regression and plotted (dotted lines). OLS regression trends and p-values are shown in the legend.

326 which visually matches their results. They deemed the trends to be statistically significant at the
 327 10% level since the intervals did not include zero. However, 90% confidence intervals for the 0.9

328 quantile trends from OLS, bootstrap pairs, and bootstrap residuals (1000 samples) are [-0.04, 0.4],
329 [-0.051, 0.45], and [-0.022, 0.4] kt yr⁻¹, respectively. These intervals are all larger than the Bhatia
330 et al. (2019) interval by more than a factor of two, and all include zero, which means that the trend
331 is statistically insignificant at the 10% level (OLS p-value = 0.17). The 90% confidence intervals
332 for the 0.95 quantile trends from OLS, bootstrap pairs, and bootstrap residuals (1000 samples) are
333 [0.015, 0.58], [0.0034, 0.6], and [0.023, 0.57] kt yr⁻¹, which are larger than the jitter-based ones by
334 nearly a factor of three. Similar considerations apply to the positive trend in RI frequency reported
335 by Bhatia et al. (2019). We found the same slope of 0.14 percentage points (pp) yr⁻¹ over the
336 period 1982–2009 (Fig. 4c) but the OLS 90% confidence interval of [0.026, 0.25] pp yr⁻¹ is wider
337 by more than a factor of two than the interval [0.1, 0.18] pp yr⁻¹ reported by Bhatia et al. (2019).
338 Adding jitter to simulate observation error fails to represent regression coefficient uncertainty.

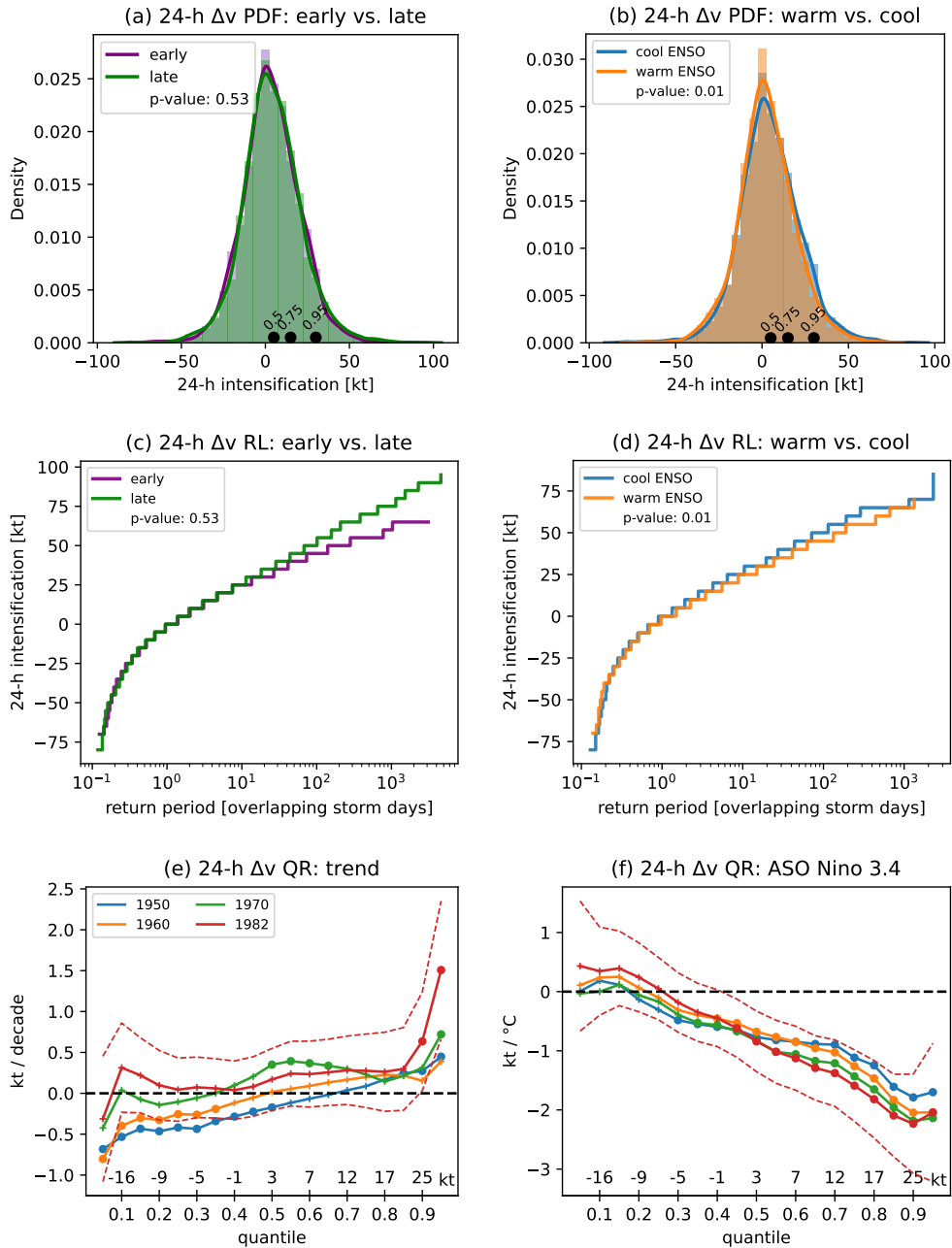
339 Another point is that examination of the 24-intensification and RI frequency timeseries suggests
340 that the trends may be specific to the choice of period. All three timeseries have higher values
341 prior to the 1982–2009 period, modest values in the 1980s, and an unusually high value in 2007
342 (strong La Niña). When the analysis period was extended to 2024, the 0.9 and 0.95 annual quantile
343 trends dropped to 0.09 kt yr⁻¹ and 0.08 kt yr⁻¹ with OLS p-values of 0.20 and 0.33, respectively.
344 Likewise, when the analysis period was extended to 2024, the RI frequency trend dropped to 0.06
345 pp yr⁻¹ and was not statistically significant (p-value = 0.104).

346 We will see in Section 4 that quantile regression (as opposed to OLS regression with annual
347 quantiles) finds significant upward intensification trends in the 0.9 and 0.95 quantiles over the
348 period 1982–2024. Similarly we will see in Section 4 that logistic regression (as opposed to OLS
349 regression of annual proportions) with time and Niño-3.4 as covariates finds significant upward
350 RI (30 kt threshold) frequency trends over the period 1982–2024. We discuss how year-to-year
351 variations in sample size is one potential reason for these different results in Section 5.

352 **4. Trends and ENSO-related variability**

353 *a. 24-h intensification*

360 We first examined trends and ENSO-related variability in Atlantic 24-h intensification values.
361 Differences in the distribution of 24-h intensification values between early and late periods are
362 statistically insignificant, and the probability density functions are visually indistinguishable (Fig.



354 FIG. 5. Histograms and kernel-smoothed probability density functions (PDFs) of Atlantic 24-h intensification
 355 (24-h Δv) 1982–2024 during (a) early and late periods and (b) warm and cool ENSO conditions. Return level
 356 (RL) curves for Atlantic 24-h intensification (1982–2024) during (c) early and late periods and (d) warm and
 357 cool ENSO conditions. Atlantic 24-h intensification quantile regression (QR) coefficients for the (e) trend and
 358 (f) Niño-3.4. Colors indicate start year shown in legend. 95% confidence intervals are shown (red dashed lines)
 359 for the 1982–2024 coefficients. Filled circles indicate statistically significant (5% level) coefficients.

363 5a). The return level curves reveal that late period intensification rates greater than 25 kt are shifted
364 toward shorter return periods, which means they occur more frequently (Fig. 5c). Differences in
365 the distribution of Atlantic 24-h intensification values between warm and cool ENSO years are
366 statistically significant, and the kernel smoothed density functions show a modest but consistent
367 shift rightward for positive 24-h intensification values during cool years (Fig. 5b). This shift in
368 cool ENSO years results in a reduction of return periods for positive 24-h intensification values,
369 and the return period reduction is larger at larger values (Fig. 5d). Quantile regression of 24-h
370 intensification with time and Niño-3.4 as covariates shows that significant trends are limited to the
371 0.9 and 0.95 quantiles (0.6 and 1.5 kt decade⁻¹, respectively) over the 1982–2024 period. Negative
372 trends in the lower quantiles are significant when the analysis start year is 1950 or 1960, but not
373 for later start years (Fig. 5e). Niño-3.4 quantile coefficients are negative and significant above the
374 0.45 quantile (positive intensification values) and decrease with increasing quantile up to the 0.9
375 quantile (2.2 kt °C⁻¹; Fig. 5f), consistent with the composite results.

376 *b. Lifetime maximum 24-h intensification*

377 LM24I is a new per storm intensification diagnostic which has not been examined previously for
378 trends or ENSO-related variability. The difference between the distributions of Atlantic LM24I
379 during early and late periods is not significant (Fig. 6a). There is a shift above 30 kt to shorter
380 return periods in the late period, and this shift is largest at the extreme right tail (Fig. 6c). In the
381 early period the largest LM24I value is 65 kt (Andrew, 1992; Keith, 2000) and in the late period it
382 is 95 kt (Wilma, 2005). The difference between the distributions of LM24I intensification in warm
383 and cool ENSO years is significant with a shift to higher values during the cool years (Figs. 6b,
384 d). This shift to higher values during cool ENSO conditions is present across nearly all values and
385 is fairly uniform. The largest LM24I value during a warm ENSO year is 70 kt (Lee, 2023), and
386 during a cool ENSO year it is 85 kt (Felix, 2007). Quantile regression of LM24I with time and
387 Niño-3.4 as covariates show that significant trends are limited to the 0.9 and 0.95 quantiles (3.5
388 and 4.8 kt decade⁻¹; Fig. 6e). Most Niño-3.4 quantile coefficients are significant (Fig. 6f) with
389 values near that of the median coefficient value of -3.3 kt °C⁻¹. The largest trend is -5.3 kt °C⁻¹
390 for the 0.95 quantile. Both sets of coefficients are fairly robust with respect to choice of start year
391 with the largest changes tending to be at the highest quantiles.

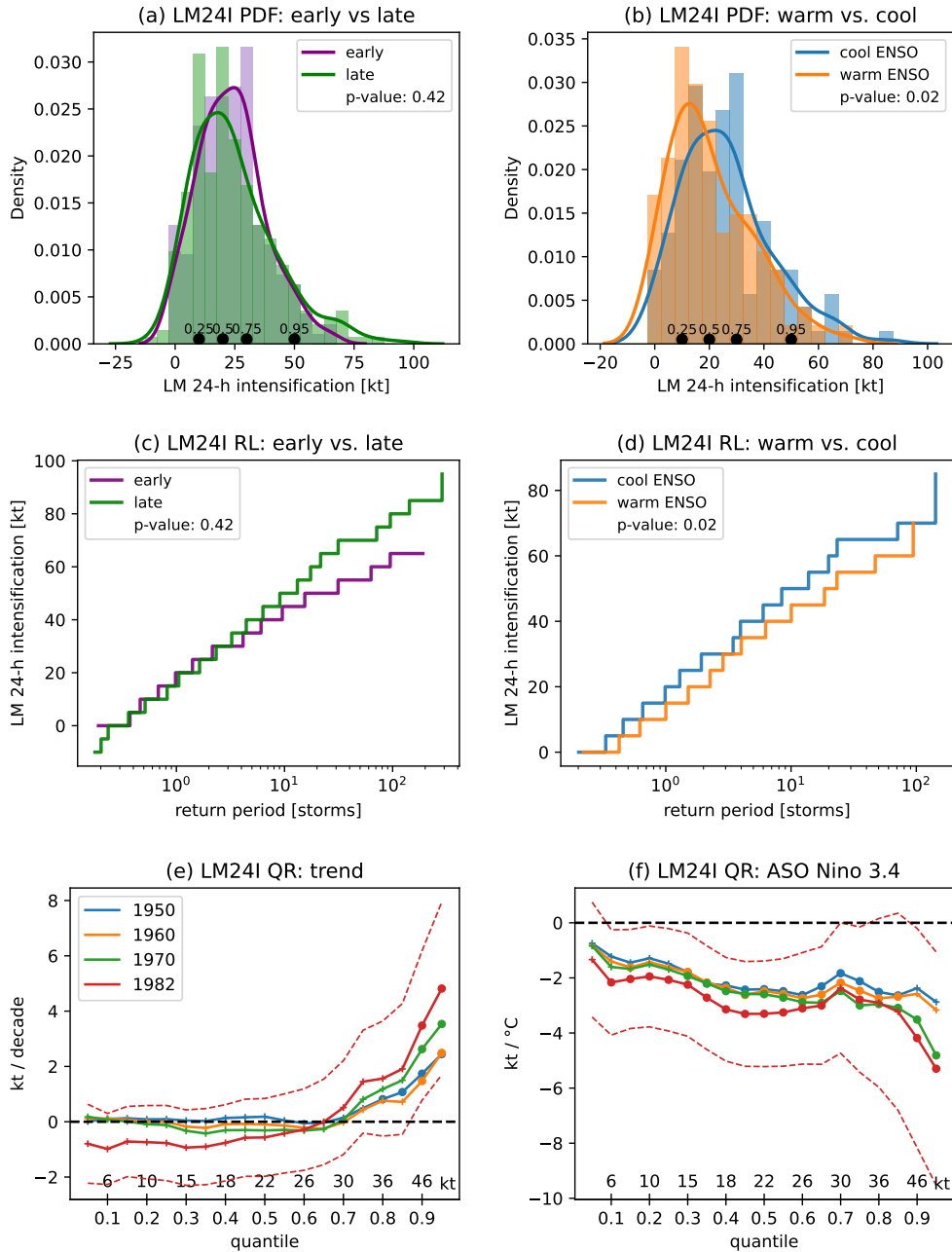
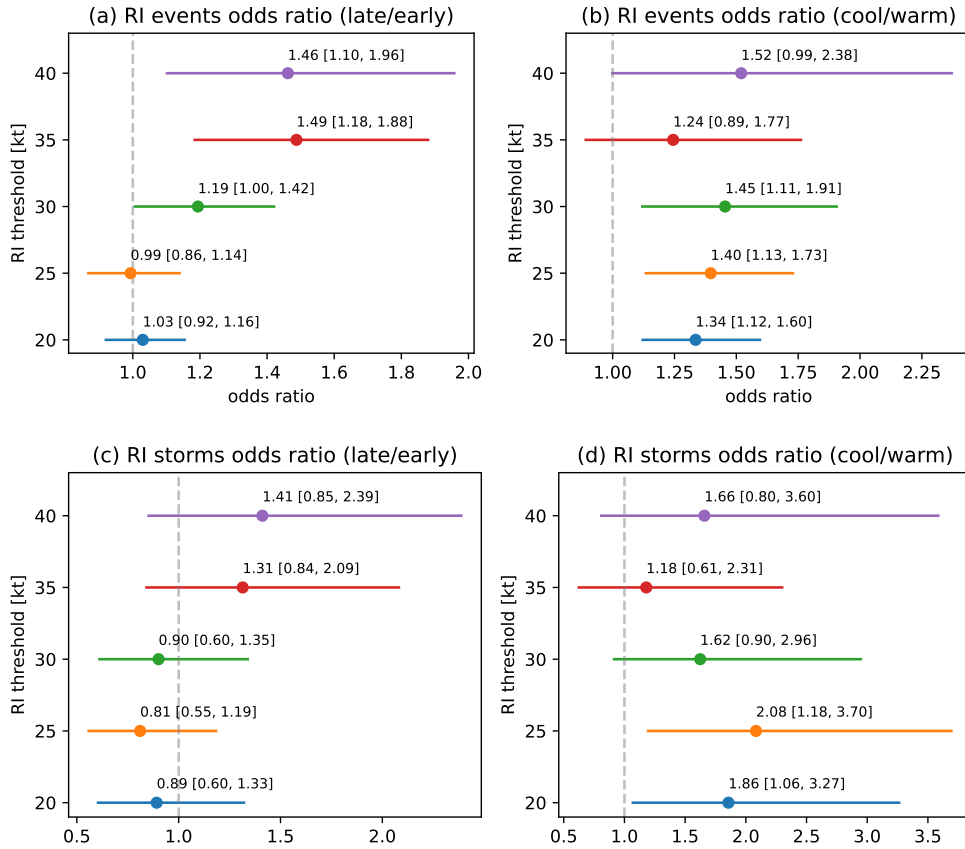


FIG. 6. As in Fig. 5 but for Atlantic lifetime maximum 24-h intensification (LM24I).

392 *c. RI event and storm frequency*

396 There are substantially more RI events per year during the late period compared to the early
 397 period at all thresholds (not shown). For instance, there are 17.6 RI events per year during the late
 398 period and 10.6 per year during the early period for the 30 kt RI threshold, which is an increase



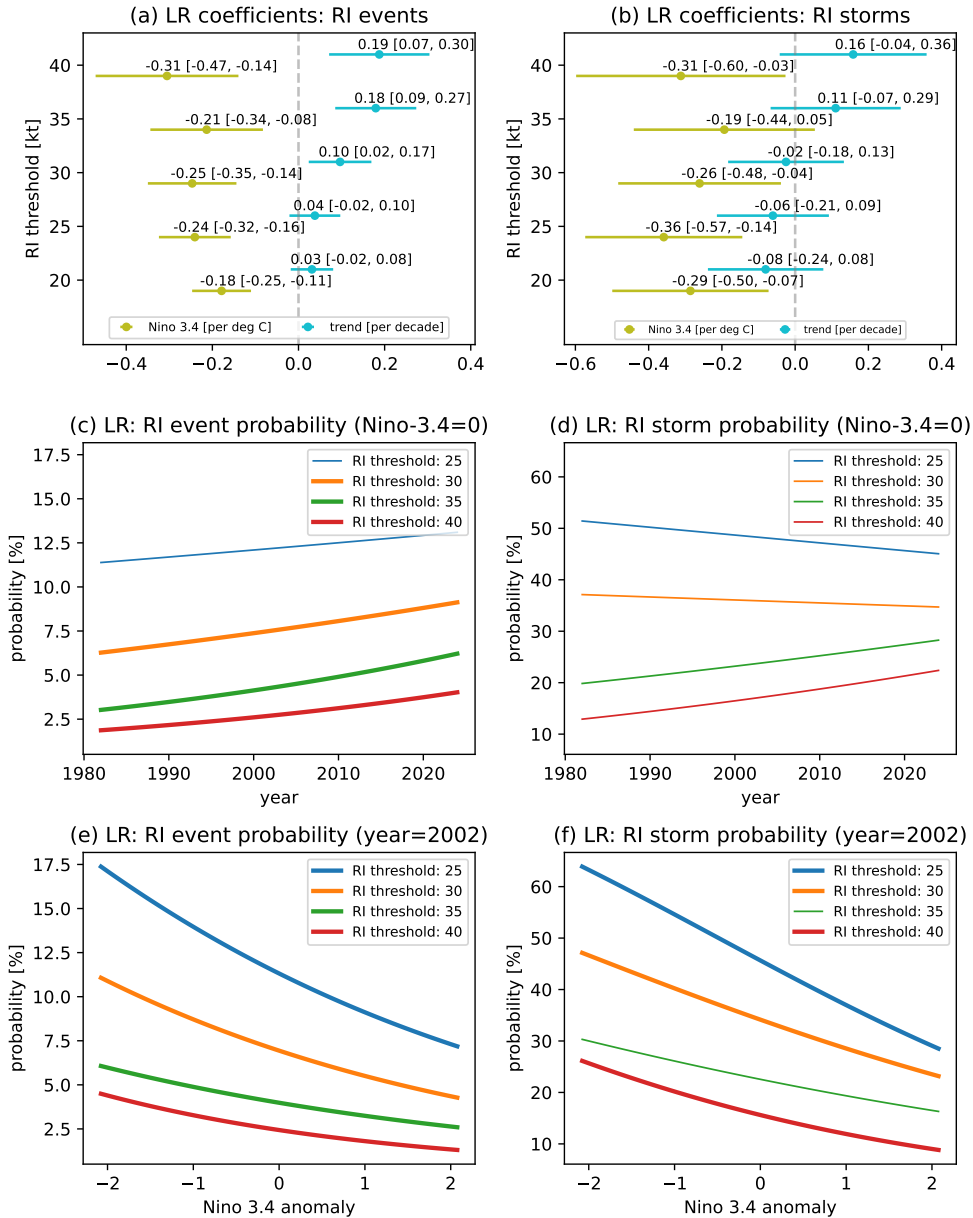
393 FIG. 7. Odds ratios (dots) with 95% confidence intervals (horizontal lines) for Atlantic RI events during (a)
 394 early vs. late periods and (b) warm vs. cool ENSO years, and for Atlantic RI storms (c) early vs. late periods and
 395 (d) warm vs. cool ENSO years for RI thresholds of 20 kt to 40 kt by 5 kt.

399 of about 66%. However, looking at RI event numbers alone fails to account for the cases when RI
 400 did not occur. In fact, there are 152 overlapping 24-h storm periods per year in the early period
 401 and 215 overlapping 24-h storm periods per year in the late period. Therefore, an increase in
 402 the number of RI events would be expected without a change in RI frequency. The odds ratio is
 403 the ratio of RI events to non-RI events. The odds ratios between early and late periods indicate
 404 significant increases in RI frequency during the late period for thresholds above 25 kt (Fig. 7a).
 405 The RI early vs. late odds ratios for thresholds of 20 kt and 25 kt are near one and are statistically
 406 insignificant. RI frequency increases at all thresholds during cool ENSO years compared with
 407 warm ENSO years, and the increase is statistically significant at thresholds below 35 kt (Fig. 7b).

408 There are more RI storms per year during the late period than during the early period at all
409 thresholds (not shown). However, there are also more storms overall (RI and non-RI) per year
410 during the late period. The odds ratio indicates that RI storm frequency decreases during the late
411 period for thresholds up to 30 kt and increases for thresholds of 35 kt and 40 kt (Fig. 7c). None
412 of the RI storm frequency changes between the early and late periods are statistically significant.
413 The number of RI storms (not shown) as well as their frequency increase during cool ENSO years
414 compared to warm ENSO years (Fig. 7d). Only the ENSO-related RI storm frequency increases at
415 20 kt and 25 kt are statistically significant at the 5% level.

422 Logistic regression shows that decreases in Niño-3.4 are accompanied by increases in the prob-
423 ability of RI events and RI storms for all RI thresholds (olive dots in in Figs. 8a, b). The
424 corresponding logistic regression coefficients are statistically significant (confidence intervals do
425 not include zero) in all cases except RI storm probability with a 35-kt threshold. The probability
426 of RI events has a positive trend for all thresholds, and the corresponding logistic regression co-
427 efficients are statistically significant for thresholds of 30 kt and above (cyan dots and lines in Fig.
428 8a). The finding of a statistically significant trend in RI frequency for threshold of 30 kt improves
429 upon the OLS analysis of annual proportions in Fig. 3 which did not find a significant trend. We
430 return to this point in Section 5. The probability of RI storms decreases with time for thresholds
431 below 35 kt and increases for thresholds of 35 kt and 40 kt, which matches the composite behavior
432 (Fig. 7c). None of the logistic regression trend coefficients for RI storms are statistically significant
433 (confidence intervals include zero; cyan lines in Fig. 8b).

434 To visualize the trends in the probability of RI events and storms, we set the Niño-3.4 anomaly to
435 zero and varied the year over its observed range 1982–2024 (Figs. 8c, d). For a RI threshold of 30
436 kt, the event probability increases from 6.3% to 9.1% ($0.07 \text{ pp decade}^{-1}$, slightly above the OLS
437 value in Fig. 4c), and the RI storm probability decreases from 37.1% to 34.7% ($-0.06 \text{ pp decade}^{-1}$).
438 Likewise, to visualize the dependence of RI event and RI storm probability on Niño-3.4, we set the
439 year to its midpoint value of 2002 and varied Niño-3.4 over its observed range (Figs. 8e, f). For a
440 RI threshold of 30, the event probability varies from from 11.1% to 4.3% ($-1.6 \text{ pp } ^\circ\text{C}^{-1} \text{ Niño-3.4}$)
441 and the storm probability varies from 47.1% to 23.2% ($-5.8 \text{ pp } ^\circ\text{C}^{-1} \text{ Niño-3.4}$). The probability of
442 RI events and RI storms over the observed range of Niño-3.4 values is larger than that from trends
443 over the period 1982–2024.



416 FIG. 8. Logistic regression (LR) coefficients (dots) for time and Niño-3.4 along with their 95% confidence
 417 intervals (horizontal lines) for the probability of (a) Atlantic RI events and (b) Atlantic RI storms. Logistic
 418 regression-fitted probability of Atlantic RI events as a function of (c) time and (e) Niño-3.4, and probability of
 419 Atlantic RI storms as a function of (d) time (f) Niño-3.4. For varying time, Niño-3.4 is fixed to its average value
 420 of zero anomaly; for varying Niño-3.4, time is fixed to its average value 2002. Fitted values with thick lines
 421 correspond to logistic regression coefficients that are statistically significant at the 5% level.

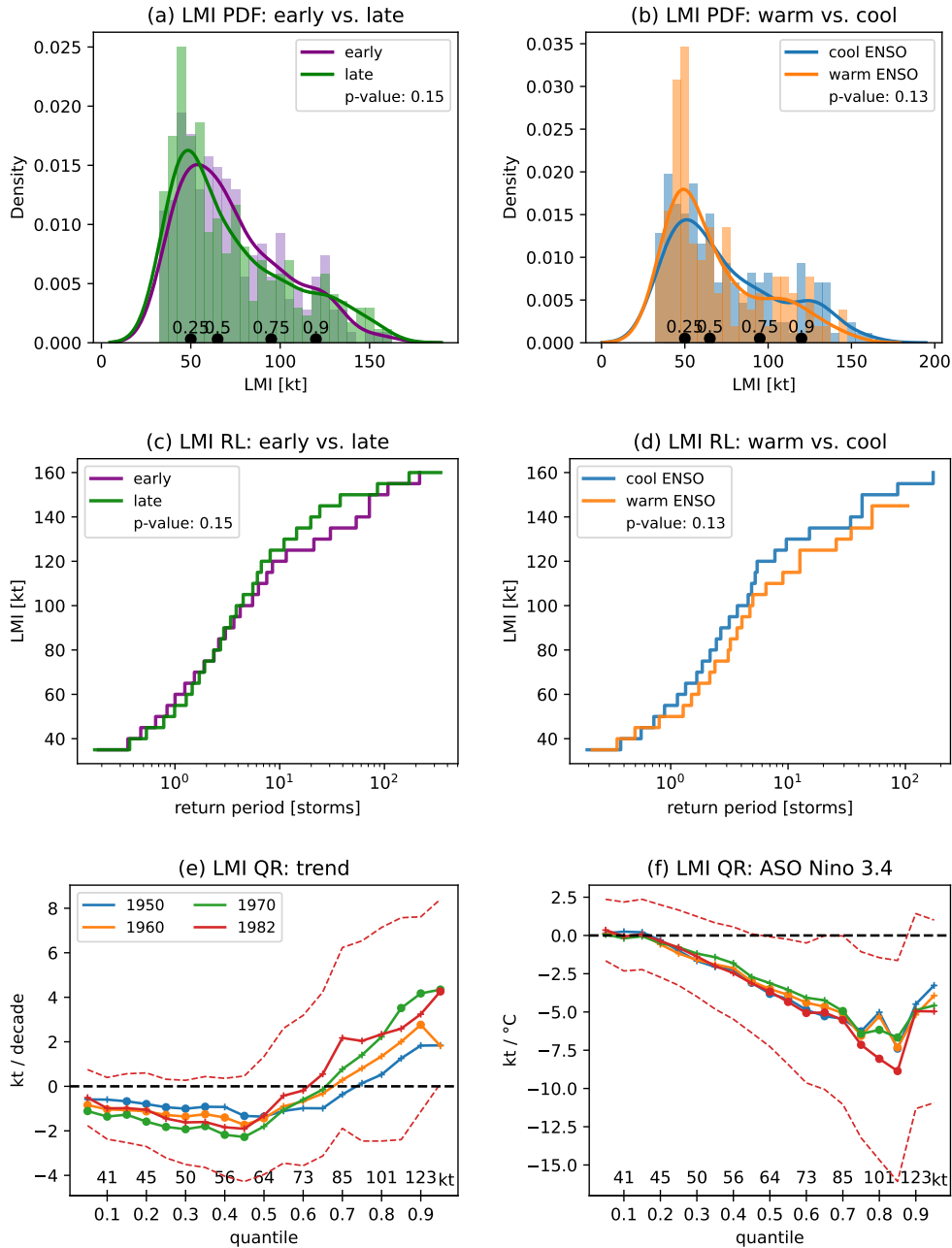


FIG. 9. As in Fig. 5 but for Atlantic lifetime maximum intensity (LMI).

444 *d. Lifetime maximum intensity*

445 Differences between the Atlantic LMI distributions in early and late periods are statistically
 446 insignificant (Fig. 9a), though this result is sensitive to the choice of period. The p-value drops to
 447 0.01 when the start year is 1980 (not shown). LMI values above 100 kt are more frequent in the late

448 period (shorter return period) and intensity values in the range of tropical storms are less frequent
449 (longer return period; Fig. 9c). The difference in Atlantic LMI distributions between warm and
450 cool ENSO years is also statistically insignificant (Fig. 9b). For LMI values above 50 kt, there is a
451 consistent shift toward shorter return periods (more frequent occurrence) during cool ENSO years
452 (Fig. 9d). Quantile regression provides a more detailed description of these distributional changes.
453 Trends in the 0.05–0.5 quantiles (tropical storm range) are negative and significant for all periods
454 except 1982–2024 (Fig. 9e). The 0.95 quantile trend of $4.3 \text{ kt decade}^{-1}$ is significant for the periods
455 1970–2024 and 1982–2024, though the significance is marginal in the sense that the lower limit of
456 the 5% confidence interval is only slightly above zero. The trend is smaller ($3.8 \text{ kt decade}^{-1}$) and
457 not significant if Niño-3.4 is removed from the quantile regression (not shown). Niño-3.4 quantile
458 coefficients are negative and significant for quantiles in the range 0.45–0.85, which corresponds to
459 Cat 1–3 hurricanes (Fig. 9f). The largest Niño-3.4 coefficient is $-8.9 \text{ kt } ^\circ\text{C}^{-1}$ for the 0.85 quantile
460 (110 kt on average).

461 **5. Summary and conclusions**

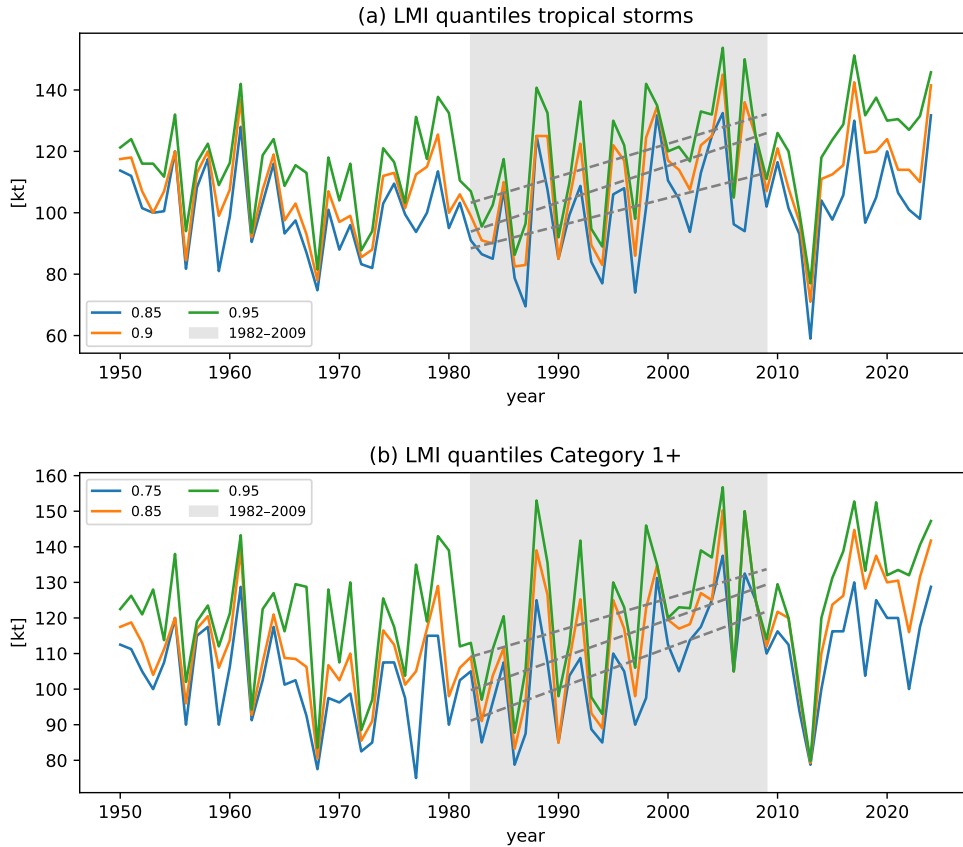
462 Here we have examined trends and ENSO-related variability in Atlantic tropical cyclone intensi-
463 ties and intensification from IBTrACS data. The quantities considered were: 24-h intensification,
464 lifetime maximum 24-h intensification (LM24I), and lifetime maximum intensity (LMI). We also
465 considered the frequency of rapid intensification (RI; 24-h intensification exceeding thresholds of
466 20 kt to 40 kt by 5 kt) and the frequency of RI storms (storms that undergo RI during their lifetime).
467 We focused on the period 1982–2024 and characterized the ENSO state by the August–October
468 Niño-3.4 index. We diagnosed trends and ENSO-related variability using composite analysis (sim-
469 ple and straightforward to interpret), quantile regression (for distributional changes), and logistic
470 regression (for frequency changes). Logistic regression for RI is common in forecast applications,
471 but its use here to assess trends and ENSO dependence in the frequency of RI events and RI storms
472 appears to be novel.

473 Significant trends in 24-h intensification are limited to the 0.9 and 0.95 quantiles with values of
474 $0.6 \text{ kt decade}^{-1}$ and $1.5 \text{ kt decade}^{-1}$, respectively. Higher trend values previously reported for the
475 period 1982–2009 might be due to unusually low and high values near the start and end of that
476 period, respectively. The modest trends isolated to the highest quantiles may be the reason that

477 composites of early and late period 24-h intensification distributions show no significant difference.
478 A new finding is that the distribution of Atlantic 24-h intensification differs significantly between
479 warm and cool ENSO years. At the quantile level, the 0.4 through 0.95 quantiles of Atlantic
480 24-h intensification (roughly the positive values) increase significantly with decreasing values of
481 Niño-3.4, about $2 \text{ kt } ^\circ\text{C}^{-1}$ of Niño-3.4 cooling at the higher quantiles. Upward trends in the high
482 quantiles of 24-h intensification would be expected to increase Atlantic RI frequency, and indeed
483 composite analysis and logistic regression show significant increases in Atlantic RI frequency over
484 time for RI thresholds of 30 kt and higher. Similarly, we found significant increases in Atlantic RI
485 frequency with decreasing values of Niño-3.4 at all RI thresholds using logistic regression. The
486 finding that Atlantic RI frequency (not only number of RI events) increases during cool ENSO
487 conditions extends the work of Klotzbach (2012, their Fig. 2) who found that more RI events occur
488 during La Niña conditions than during El Niño conditions.

489 Trends in the frequency of Atlantic RI storms are mixed. Trends are negative for RI thresholds
490 up to 30 kt and positive for thresholds of 35 and 40 kt, but none are statistically significant. The
491 ENSO relation with RI storm frequency is negative for all RI thresholds. Composite analysis finds
492 that the increase in RI storm frequency during cool ENSO conditions is statistically significant
493 for RI thresholds of 25 kt and 30 kt, while logistic regression finds they are significant at all RI
494 thresholds except 35 kt. As an alternative to the yes/no threshold-dependent RI storm classification,
495 we introduced a new per storm intensification metric called lifetime maximum 24-h intensification
496 (LM24I). Similar to 24-h intensification, we found significant positive trends in its 0.9 and 0.95
497 quantiles, though with larger values, $3\text{--}5 \text{ kt decade}^{-1}$, perhaps because LM24I is a maximum over
498 storm lifetime. We found significant changes in the Atlantic LM24I distribution between warm
499 and cool ENSO years, as well as significant increases of $2\text{--}5 \text{ kt}$ across most quantiles for each $^\circ\text{C}$
500 of Niño-3.4 cooling.

501 We found negative trends in Atlantic LMI quantiles below the median (tropical storm strength)
502 whose statistical significance varied with period. Positive trends in the 0.95 quantile (4.3 kt
503 decade^{-1}) are significant over the periods 1970–2024 and 1982–2024. The LMI trends that we
504 found here are smaller than the $15.6 \text{ kt decade}^{-1}$ ($8 \text{ m s}^{-1} \text{ decade}^{-1}$) that Kossin et al. (2013) found
505 in Atlantic storms with LMI over 65 kt over the period 1982–2009. The difference in LMI trend
506 estimates may reflect sensitivity to period since LMI values for both tropical storms and Category



513 FIG. 10. Annual quantiles (probability level in legend) of Atlantic LMI 1950–2024 for (a) tropical storms and
 514 (b) storms rated Category 1+. Values during the period 1982–2009 (shaded) are fit to a linear trend by OLS
 515 regression and the trend lines are plotted.

507 1+ hurricanes were low around 1982 and show little upward trend after 2009 (Fig. 10). A new
 508 finding is that the 0.45 to 0.85 quantiles of Atlantic LMI (roughly Category 1–3 hurricanes) have
 509 a significant negative relation with Niño-3.4 that reaches $-8.9 \text{ kt } ^\circ\text{C}^{-1}$ for the 0.85 quantile. No
 510 LMI trends are significant over the period 1982–2024 when Niño-3.4 is removed from the quantile
 511 regression, which supports the argument that accounting for ENSO variability can improve trend
 512 estimates.

516 An important methodological point which seems to have received little attention previously
 517 is that statistical analysis of best-track intensity data can be improved by adding jitter (small
 518 random numbers). Best-track intensity data are rounded to the nearest 5 kt, which can lead to
 519 poor performance of statistical methods that assume continuous distributions. Here we used jitter

520 consisting of random numbers uniformly distributed on the interval ± 2.5 kt, which fills in the gaps
521 in the data. Experiments with synthetic data demonstrated that 5 kt rounding increases the error of
522 quantile estimates and that suitable jitter decreases the error. We also showed that without jitter,
523 quantile regression may be unstable and give incorrect confidence intervals. However, the purpose
524 of adding jitter is not to compute uncertainty or statistical significance. We established here that the
525 jitter-based uncertainty quantification procedure of Bhatia et al. (2019) produces biased quantile
526 estimates and overestimates the statistical significance of trends.

527 Comparing the results here with some prior ones that we repeated here provided an opportunity to
528 compare OLS regression of annual values with logistic and quantile regression. One key difference
529 is that OLS regression of annual values (proportions or quantiles) fails to account for the number
530 of events that go into the calculation of the annual value. As an extreme illustration of this point,
531 consider RI events in 1990 and 1991 when RI occurred in 1 out of 205 24-h periods and in 5 out of
532 54 24-h periods, respectively. An intercept-only regression estimates the average frequency, and
533 logistic regression gives the correct average frequency for these two years as $(1 + 5)/(205 + 54) =$
534 2.3% . On the other hand, using annual proportions gives $(1/205 + 5/54)/2 = 4.9\%$, which can be
535 interpreted as giving too much weight to the year 1991 which has relatively few samples. We saw
536 two cases where this difference seemed to impact significance results. First, logistic regression
537 found a significant positive trend in Atlantic RI frequency 1982–2024 but OLS regression of annual
538 proportions did not (compare Figs. 4c and 8a). The trend-only logistic regression is also significant
539 (not shown) which suggests the difference is due to the differing regression methods, not the
540 inclusion of Niño-3.4. We speculate that the varying number of events from year to year might
541 play a role. The years 1991 and 2013 were inactive ones with relatively few RI opportunities, less
542 than 50% of average. However, their annual RI proportions, 29% and 0%, respectively, were in
543 opposition to an upward trend. OLS regression weights these years more than logistic regression
544 does, which might lead to the OLS trend being insignificant. The OLS trend is significant when
545 those two years are removed. Second, the OLS regression of the 0.9 and 0.95 annual quantiles of
546 24-h intensification found that the 1982–2024 trends were insignificant (Figs. 4a, b), but quantile
547 regression found the trends to be significant (Fig. 5). The same consideration about unequal
548 weighting applies to quantile regression. In this case, the trend-only quantile regression finds the

549 0.95 quantile trend significant but including Niño-3.4 in the regression is required to obtain the
550 (marginal) significance of the 0.9 quantile.

551 The findings here suggest several directions for future work. Similar analysis could be applied
552 to global intensity data and to intensity data from other basins. Previous work has found different
553 trends (Balaguru et al. 2018) and ENSO dependence in RI (Klotzbach 2012) in different Atlantic
554 sub-basins. The analysis here could be applied at sub-basin scale. An interesting question is
555 whether models simulate the same trends and ENSO relations as seen in observations. Although
556 models have limitations, especially related to intensity, their deficiencies are distinct from the ones
557 in best-track data. Model experiments could also address the issue of attributing trends (Murakami
558 2022). Although ENSO forecast skill is relatively low for August–October targets (e.g., Fig.
559 10.3 of L'Heureux et al. 2020), ENSO forecasts could potentially be translated into intensity
560 predictions. We have used the Niño-3.4 index to characterize the ENSO state, but relative Niño-3.4
561 which removes the tropical mean SST might provide a better measure of ENSO teleconnections
562 in a warming climate (Van Oldenborgh et al. 2021; L'Heureux et al. 2024). Future work should
563 consider trends and ENSO-related variability in tropical cyclone intensity as measured by surface
564 pressure (Klotzbach et al. 2020).

565 This study has tried to avoid some of the problems of best-track intensity data by addressing
566 5 kt discretization, focusing on the period during which satellite data are available, and limiting
567 our attention to a single basin and data-providing agency, but there might be other data issues that
568 could impact the results. For instance, data quality may vary over time, which has not been taken
569 into account here. This issue might impact analysis of trends more directly than analysis of ENSO
570 variability.

571 *Acknowledgments.* SJC acknowledges support from NSF (AGS-2043142, AGS-2217618, and
572 AGS-224491), NOAA (NA21OAR430345, NA22OAR4310610) and DOE (DE-SC0023333).

573 *Data availability statement.* North Atlantic International Best Track Archive for Cli-
574 mate Stewardship data was downloaded from [https://www.ncei.noaa.gov/data/
575 international-best-track-archive-for-climate-stewardship-ibtracs/v04r01/
576 access/csv/ibtracs.NA.list.v04r01.csv](https://www.ncei.noaa.gov/data/international-best-track-archive-for-climate-stewardship-ibtracs/v04r01/access/csv/ibtracs.NA.list.v04r01.csv). NOAA Extended Reconstructed SST
577 V5 data provided by the NOAA PSL, Boulder, Colorado, USA, from their website at
578 <https://downloads.psl.noaa.gov/Datasets/noaa.ersst.v5/sst.mmmean.nc>.

579 **References**

580 Balaguru, K., G. R. Foltz, and L. R. Leung, 2018: Increasing magnitude of hurricane rapid
581 intensification in the central and eastern tropical Atlantic. *Geophysical Research Letters*, **45**,
582 4238–4247.

583 Balaguru, K., G. R. Foltz, L. R. Leung, W. Xu, D. Kim, H. Lopez, and R. West, 2022: Increasing
584 hurricane intensification rate near the US Atlantic coast. *Geophysical Research Letters*, **49**,
585 e2022GL099793.

586 Barnston, A. G., M. Chelliah, and S. B. Goldenberg, 1997: Documentation of a highly ENSO-
587 related SST region in the equatorial Pacific. *Atmosphere-Ocean*, **35**, 367–383.

588 Becker, E. J., and M. K. Tippett, 2024: Impact of ENSO and trends on the distribution of North
589 American wintertime daily temperature. *Journal of Climate*, **37**, 3509–3520, [https://doi.org/
590 https://doi.org/10.1175/JCLI-D-23-0569.1](https://doi.org/10.1175/JCLI-D-23-0569.1).

591 Bhatia, K., and Coauthors, 2022: A potential explanation for the global increase in tropical cyclone
592 rapid intensification. *Nature Communications*, **13**, 6626.

593 Bhatia, K. T., G. A. Vecchi, T. R. Knutson, H. Murakami, J. Kossin, K. W. Dixon, and C. E. Whit-
594 lock, 2019: Recent increases in tropical cyclone intensification rates. *Nature Communications*,
595 **10**, 1–9.

596 Bove, M. C., J. B. Elsner, C. W. Landsea, X. Niu, and J. J. O'Brien, 1998: Effect of El Niño
597 on US landfalling hurricanes, revisited. *Bulletin of the American Meteorological Society*, **79**,
598 2477–2482.

599 Camargo, S. J., and Coauthors, 2023: An update on the influence of natural climate variability and
600 anthropogenic climate change on tropical cyclones. *Tropical Cyclone Research and Review*, **12**,
601 216–239.

602 DelSole, T. M., and M. K. Tippett, 2022: *Statistical Methods for Climate Scientists*. Cambridge
603 University Press, <https://doi.org/10.1017/9781108659055>.

604 Elsner, J. B., and T. H. Jagger, 2013: Intensity models. *Hurricane Climatology: A Modern
605 Statistical Guide Using R*, Oxford University Press, [https://doi.org/10.1093/oso/9780199827633.](https://doi.org/10.1093/oso/9780199827633.003.0012)
606 003.0012.

607 Gahtan, J., K. R. Knapp, C. J. Schreck, H. J. Diamond, J. P. Kossin, and M. C. Kruk, 2024:
608 International Best Track Archive for Climate Stewardship (IBTrACS) Project, Version 4r01.
609 NOAA, <https://doi.org/10.25921/82ty-9e16>.

610 Gray, W. M., 1984: Atlantic Seasonal Hurricane Frequency. Part I: El Niño and 30 mb Quasi-
611 Biennial Oscillation Influences. *Monthly Weather Review*, **112**, 1649–1668.

612 Hanley, D. E., M. A. Bourassa, J. J. O'Brien, S. R. Smith, and E. R. Spade, 2003: A quantitative
613 evaluation of ENSO indices. *Journal of Climate*, **16**, 1249–1258.

614 Huang, B., and Coauthors, 2017: Extended reconstructed sea surface temperature, version 5
615 (ERSSTv5): Upgrades, validations, and intercomparisons. *Journal of Climate*, **30**, 8179–8205,
616 <https://doi.org/10.1175/JCLI-D-16-0836.1>.

617 Jagger, T. H., and J. B. Elsner, 2009: Modeling tropical cyclone intensity with quantile regression.
618 *International Journal of Climatology: A Journal of the Royal Meteorological Society*, **29**,
619 1351–1361.

620 Klotzbach, P. J., 2011: El Niño–Southern Oscillation's impact on Atlantic basin hurricanes and
621 US landfalls. *Journal of Climate*, **24**, 1252–1263.

622 Klotzbach, P. J., 2012: El Niño-Southern Oscillation, the Madden-Julian Oscillation and Atlantic
623 basin tropical cyclone rapid intensification. *Journal of Geophysical Research: Atmospheres*,
624 **117**, D14 104.

625 Klotzbach, P. J., M. M. Bell, S. G. Bowen, E. J. Gibney, K. R. Knapp, and C. J. Schreck, 2020:
626 Surface pressure a more skillful predictor of normalized hurricane damage than maximum
627 sustained wind. *Bulletin of the American Meteorological Society*, **101**, E830–E846.

628 Klotzbach, P. J., K. M. Wood, C. J. Schreck III, S. G. Bowen, C. M. Patricola, and M. M. Bell,
629 2022: Trends in global tropical cyclone activity: 1990–2021. *Geophysical Research Letters*, **49**,
630 e2021GL095 774.

631 Knaff, J. A., C. R. Sampson, and K. D. Musgrave, 2018: An operational rapid intensification
632 prediction aid for the western North Pacific. *Weather and Forecasting*, **33**, 799–811.

633 Knapp, K. R., M. C. Kruk, D. H. Levinson, H. J. Diamond, and C. J. Neumann, 2010: The
634 International Best Track Archive for Climate Stewardship (IBTrACS). *Bulletin of the American
635 Meteorological Society*, **91**, 363–376.

636 Knutson, T., and Coauthors, 2019: Tropical cyclones and climate change assessment: Part I:
637 Detection and attribution. *Bulletin of the American Meteorological Society*, **100 (10)**, 1987–
638 2007.

639 Knutson, T., and Coauthors, 2020: Tropical cyclones warming world: An assessment of projec-
640 tions. *Bulletin of the American Meteorological Society*, **101**, 771–774.

641 Knutson, T. R., and Coauthors, 2010: Tropical cyclones and climate change. *Nature geoscience*,
642 **3**, 157–163.

643 Koenker, R., and G. Bassett, 1978: Regression quantiles. *Econometrica*, **46**, 33–50.

644 Kossin, J. P., T. L. Olander, and K. R. Knapp, 2013: Trend analysis with a new global record of
645 tropical cyclone intensity. *Journal of Climate*, **26**, 9960–9976.

646 Lee, C.-Y., M. K. Tippett, A. H. Sobel, and S. J. Camargo, 2016: Rapid intensification and
647 the bimodal distribution of tropical cyclone intensity. *Nature Communications*, **7**, 10 625,
648 <https://doi.org/10.1038/ncomms10625>.

649 L'Heureux, M. L., and Coauthors, 2024: A relative sea surface temperature index for classifying
650 ENSO events in a changing climate. *Journal of Climate*, **37**, 1197–1211, [https://doi.org/10.1175/
651 JCLI-D-23-0406.1](https://doi.org/10.1175/JCLI-D-23-0406.1).

652 L'Heureux, M. L., A. Levine, M. Newman, C. Ganter, J.-J. Luo, M. K. Tippett, and T. Stock-
653 dale, 2020: ENSO Prediction. *El Niño-Southern Oscillation (ENSO) in a Changing Climate*,
654 M. McPhaden, A. Santoso, and W. Cai, Eds., AGU.

655 Machado, J., and J. Silva, 2005: Quantiles for counts. *J. Am. Stat. Assoc.*, **100**, 1226–1237.

656 Murakami, H., 2022: Substantial global influence of anthropogenic aerosols on tropical cyclones
657 over the past 40 years. *Science advances*, **8**, eabn9493.

658 Pearson, E. S., 1950: On questions raised by the combination of tests based on discontinuous
659 distributions. *Biometrika*, **37**, 383–398.

660 Sobel, A. H., S. J. Camargo, T. M. Hall, C.-Y. Lee, M. K. Tippett, and A. A. Wing, 2016: Human
661 influence on tropical cyclone intensity. *Science*, **353**, 242–246, [https://doi.org/10.1126/science.
662 aaf6574](https://doi.org/10.1126/science.aaf6574).

663 Tang, B. H., and J. Neelin, 2004: ENSO influence on Atlantic hurricanes via tropospheric warming.
664 *Geophysical Research Letters*, **31**, L24 204, <https://doi.org/10.1029/2004GL021072>.

665 Tippett, M. K., C. Lepore, and J. E. Cohen, 2016: More tornadoes in the most extreme U.S. tornado
666 outbreaks. *Science*, **354**, 1419–1423, <https://doi.org/10.1126/science.aah7393>.

667 Van Oldenborgh, G. J., H. Hendon, T. Stockdale, M. L'Heureux, E. C. De Perez, R. Singh, and
668 M. Van Aalst, 2021: Defining El Niño indices in a warming climate. *Environmental Research
669 Letters*, **16**, 044 003.

670 Wang, C., X. Wang, R. H. Weisberg, and M. L. Black, 2017: Variability of tropical cyclone
671 rapid intensification in the North Atlantic and its relationship with climate variations. *Climate
672 Dynamics*, **49**, 3627–3645.

673 Williams, I. N., and C. M. Patricola, 2018: Diversity of ENSO events unified by convective
674 threshold sea surface temperature: A nonlinear ENSO index. *Geophysical Research Letters*, **45**,
675 9236–9244.

676 Zhai, A. R., and J. H. Jiang, 2014: Dependence of US hurricane economic loss on maximum wind
677 speed and storm size. *Environmental Research Letters*, **9**, 064 019.